Antiproton compression and radial measurements

G.B. Andresen*, W. Bertsche†, P.D. Bowe*, C.C. Bray**, E. Butler†, C.L. Cesar‡, S. Chapman**, M. Charlton†, J. Fajans**, M.C. Fujiwara§, R. Funakoshi¶, D.R. Gill§, J.S. Hangst*, W.N. Hardy∥, R.S. Hayano¶, M.E. Hayden††, A.J. Humphries†, R. Hydomako‡‡, M.J. Jenkins†, L.V. Jørgensen†, L. Kurchaninov§, R. Lambo‡, N. Madsen†, P. Nolan§§, K. Olchanski§, A. Olin§, R.D. Page§§, A. Povilus**, P. Pusa§§, F. Robicheaux¶¶, E. Sarid***, S. Seif El Nasr∥, D.M. Silveira‡, J.W. Storey§, R.I. Thompson‡‡, D.P. van der Werf†, J.S. Wurtele** and Y. Yamazaki†††

*Department of Physics and Astronomy, Aarhus University, DK-8000 Aarhus C, Denmark
†Department of Physics, Swansea University, Swansea SA2 8PP, United Kingdom
**Department of Physics, University of California at Berkeley, Berkeley, CA 94720-7300, USA
‡Instituto de Física, Universidade Federal do Rio de Janeiro, Rio de Janeiro 21941-972, Brazil
§TRIUMF, 4004 Wesbrook Mall, Vancouver BC, Canada V6T 2A3
¶Department of Physics, University of Tokyo, Tokyo 113-0033, Japan
∥Department of Physics and Astronomy, University of British Columbia, Vancouver BC, Canada V6T 1Z4
††Department of Physics, Simon Fraser University, Burnaby BC, Canada V5A 1S6
‡‡Department of Physics and Astronomy, University of Calgary, Calgary AB, Canada T2N 1N4
§§Department of Physics, University of Liverpool, Liverpool L69 7ZE, United Kingdom
¶¶Department of Physics, Auburn University, Auburn, AL 36849-5311, USA
***Department of Physics, NRCN-Nuclear Research Center Negev, Beer Sheva, IL-84190, Israel
†††Atomic Physics Laboratory, RIKEN, Saitama 351-0198, Japan

Abstract. Control of the radial profile of trapped antiproton clouds is critical to trapping antihydrogen. We report detailed measurements of the radial manipulation of antiproton clouds, including areal density compressions by factors as large as ten, achieved by manipulating spatially overlapped electron plasmas. We show detailed measurements of the near-axis antiproton radial profile, and its relation to that of the electron plasma. We also measure the outer radial profile by ejecting antiprotons to the trap wall using an octupole magnet.

Keywords: Antihydrogen, Antiprotons, Rotating Wall, Radial Profile
PACS: 36.10.Ðk, 34.80.Lx, 52.20.Hv

INTRODUCTION

The current generation of antihydrogen experiments [1, 2] aims to trap $\overline{H}$ atoms. Neutral $\overline{H}$ atoms have a small permanent magnetic moment, and can be trapped in a magnetic minimum. Traps based on this effect are called Minimum-B traps [3]. To trap both charged and neutral species simultaneously, Minimum-B and Penning-Malmberg traps must be co-located. The compatibility of Minimum-B and Penning-Malmberg traps remains controversial [4, 1, 2], but it is clear that the two are most compatible if the
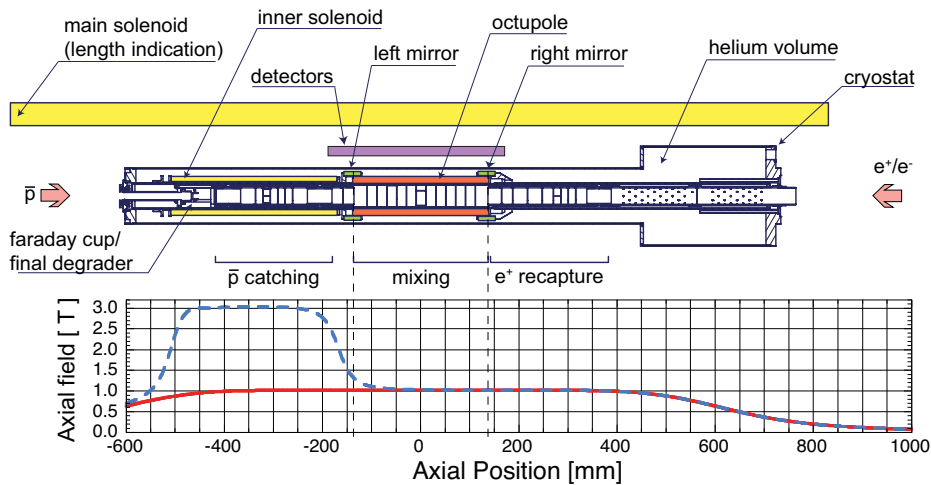
FIGURE 1. Schematic diagram of the ALPHA apparatus. A moveable probe on the right alternately inserts an electron gun and a MCP/Phosphor assembly. The graph below the schematic plots the axial magnetic field in the trap; the dashed line includes the field of the inner solenoid, while the solid line is the field without the inner solenoid.

$\bar{p}$'s and e^+'s are held close to the trap axis where the perturbations from the Minimum-B fields are smallest [5, 6, 7]. This minimizes fast (due to ballistic processes) and slow (due to diffusion) losses from the trap. Minimizing the slow losses also reduces the temperature of the $\bar{p}$'s, as slow charged particle expansion converts self-electrostatic energy into kinetic energy. Keeping the $\bar{p}$'s close to the axis also helps make the $\bar{H}$ that is synthesized more trapable. It reduces the islanding [6] which occurs as $\bar{p}$'s bounce back and forth, and can disrupt the collisional cooling of the $\bar{p}$'s on electron plasmas, thereby keeping the $\bar{H}$'s warm. It slows the $\mathbf{E} \times \mathbf{B}$ drifts of the $\bar{p}$'s which increase the kinetic energy of the $\bar{H}$'s that form from the $\bar{p}$'s, and can make the $\bar{H}$'s impossible to confine in the very shallow Minimum-B traps. Finally, it assures that any $\bar{H}$ that is synthesized is created very near the trap's minimum magnetic field, thereby retaining the maximum possible trap depth.

Successful $\bar{p}$ compression has been briefly reported elsewhere [8, 9, 10]; here we present carefully controlled and quantitative characterization of the process [11], as well as accurate measurements of the near-axis radial distribution of the $\bar{p}$'s. We have demonstrated areal density increases by as much as a factor of ten, and have produced $\bar{p}$ clouds with radii as small as 0.29 ± 0.06 mm. Clouds of this size are far from the loss limits [5] of our combined trap [1], and promise to be much easier to confine.

A schematic drawing of our apparatus is shown in Fig 1. The experiment synthesizes $\bar{H}$ using the well-known procedures pioneered by the ATHENA [12] and ATRAP [13] collaborations. Of special note here is the electron plasma used to cool the antiprotons [14] in the "$\bar{p}$ catching" section of the trap, and the octupole in the "mixing" (Minimum-B) section of the trap.

97
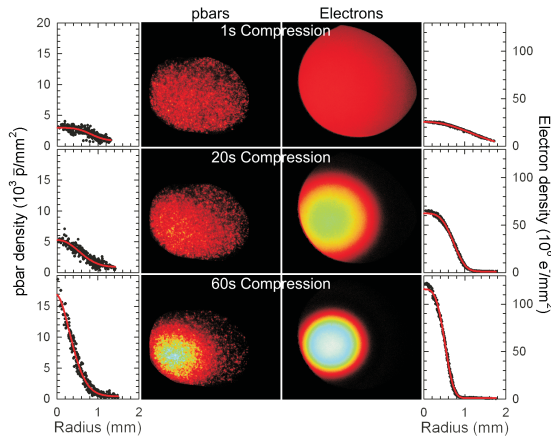
FIGURE 2. $\bar{p}$ and e^- images showing the effects of compression, and the resulting radial profiles. The red lines are Gaussian-like (i.e. $\exp(-|r/r_0|^k)$, where $k \approx 2$) fits to the radial profiles. The sharp boundaries are caused by apertures.

IMAGING

We image (see Fig. 2) the e^-'s and $\bar{p}$'s by allowing them to escape along the magnetic field lines onto a microchannel plate (MCP)/phosphor screen assembly. We capture the resultant images with a CCD camera [15]. Some typical images are shown in Fig. 2. As the MCP is in a B-field of 0.024 T, which is much lower than the trap field of 3 T, the cross-sectional area covered by the particles expands by a factor of 125 as they follow the field lines to the MCP. The details of the expansion process, as well as the brightness calibration of the image, will be described in a forthcoming paper.

ROTATING WALL

The radial size of the electron plasma used to cool the incoming $\bar{p}$'s can be controlled by applying a rotating electrostatic potential to the plasma [16, 17]. By varying the size of this plasma we find, as expected, that the size of the resulting $\bar{p}$ cloud scales with the size of the e^- plasma (see Fig. 3). Moreover the fraction of the trapped $\bar{p}$'s that are cooled (the cooling efficiency) also increases with the size of the e^- plasma [9]. This result is consistent with the model that $\bar{p}$'s do not make large radial excursions, and cool only if they traverse regions of high e^- density.

COMPRESSION

As shown in Fig. 3, we have to use a fairly large radius e^- plasma to cool the majority of the initially captured $\bar{p}$'s. Such a large radius plasma is fatter than we would like for injecting into our octupole magnet. Consequently, we would prefer to start with a large
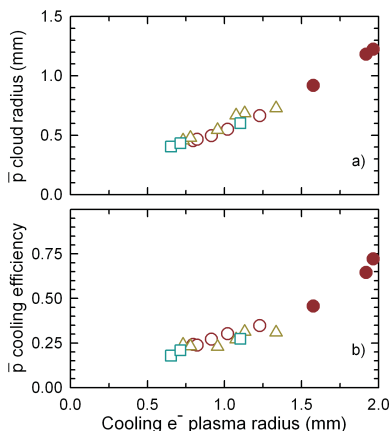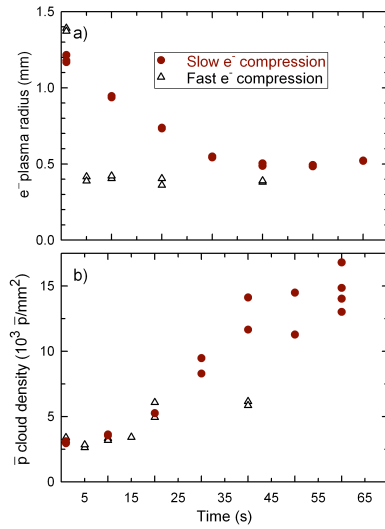
FIGURE 3. a) The cooled $\bar{\text{p}}$ cloud radius as a function of the radius of the e^- plasma. The various symbols correspond to trials with differing total electron numbers (100-165 M). b) The cooling efficiency (see text) as a function of the e^- plasma radius.

radius e^- plasma to maximize cooling, and compress the $\bar{\text{p}}$'s after cooling to optimize injection. We can accomplish this by compressing a mixed e^-–$\bar{\text{p}}$ plasma with a rotating electrostatic potential. Images of typical results are shown in Fig. 2. We observe (Figs. 4 and 5) that, so long as we compress slowly, the radius of the $\bar{\text{p}}$'s tracks that of the e^-'s. We have observed compressions as large as a factor of ten; the data series in Fig. 4 shows compression by a factor of five. We do not get compression for a pure $\bar{\text{p}}$ plasma. This is likely because the rotating wall technique is presumed to require a cooling mechanism; no such mechanism exists for a pure $\bar{\text{p}}$ plasma. We note, however, that the ASACUSA group does obtain compression of some of their $\bar{\text{p}}$'s in pure $\bar{\text{p}}$ plasmas [8, 9, 10]. Their results are hard to reconcile with ours.

OUTER RADIAL PROFILE MEASUREMENTS

Our MCP diagnostic only images $\bar{\text{p}}$'s that are near the trap axis. While the $\bar{\text{p}}$ clouds that are best for synthesizing and trapping $\overline{\text{H}}$ lie in the imaged region, it is very useful, for diagnostic purposes, to be able to determine the profile of $\bar{\text{p}}$ clouds that extend well outside the imaged region. We can find the profile of such clouds using our octupole magnet [18]. To understand how this diagnostic works, it is helpful to visualize the field lines generated by the solenoid and octupole coils. The field lines originating from a circular locus of points in the plane transverse to the solenoid axis form a four-fluted cylindrical surface; the flutes at each end are rotated by 45° with respect to each other (Fig. 6). Figure 7 shows an image of one quadrant of the field lines, generated by passing e^-'s through the octupole and onto our MCP/Phosphor screen [11].

Antiprotons confined by the electrostatic well within the octupole bounce back and forth while following the magnetic field lines. Antiprotons on field lines that extend to

99

FIGURE 4. The a) e$^-$ radius and b) $\bar{p}$ density as a function of time, for fast and slow compression. Note that the $\bar{p}$ density does not track the e$^-$ compression if the latter is fast.
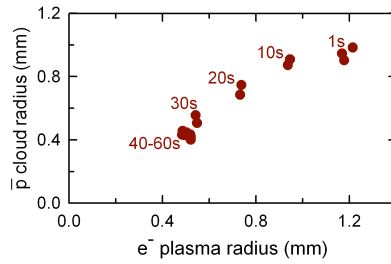

FIGURE 5. The $\bar{p}$ cloud radius as a function of the e$^-$ plasma radius for the slow compression data shown in Fig. 4.

the physical trap wall at R_w before reaching one of the electrostatic walls will follow them there and annihilate. For a given end-to-end bounce length L, field lines lying outside of a critical radius r_c at the trap center will hit the wall, while those lying inside the critical radius will not. The normalized critical radius is [5, 19]:

$$\frac{r_c}{R_w} = \frac{1}{\sqrt{1 + \frac{B_w}{B_z}\frac{L}{R_w}}},$$

(1)

where B_w is the octupole strength at the wall, and B_z is the solenoid field strength. The longer the trap, and the stronger the octupole field, the smaller the critical radius. The normalized critical radius is never smaller than about 7 mm for our magnets and wells

100
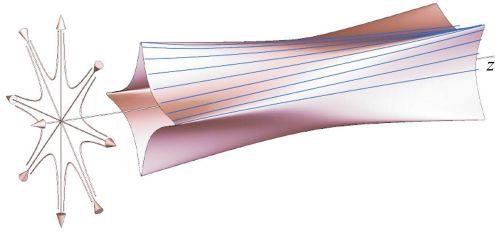
FIGURE 6. Magnetic field generated by the octupole and solenoid coils. The vectors on the left represent the directions of the axially-invariant field from these coils. The surface is created by following the field lines from a radially centered circular locus of points; the lines shown within the surface are field lines.

because the octupole field, which scales as r^3/R_w^3, is very weak near the trap axis relative to its strength at the wall.

The ballistic loss of particles on trap walls in the presence of a multipole field was first identified with electrons in a quadrupole magnet [4]. This process is easier to study with $\bar{p}$'s than with e^-'s, however, because individual $\bar{p}$ annihilations can be detected and localized on the trap wall with a position sensitive detector. The detector [20] comprises three layers of silicon cylindrically arrayed around the trap axis just outside of the octupole magnet (see Fig. 1). It is not yet fully deployed, but, using a partial system consisting of 10% of the full system, we observe (Fig. 8) that $\bar{p}$'s hit the wall at the ends of the electrostatic well. We expect to observe this type of loss pattern, as it is at the ends of the trap that the accessible field lines extend furthest outward; we note, however, that annihilations tend to occur at the ends of the electrostatic well even in the absence of an octupole field [21].

For the experiments reported here, annihilations were detected by scintillators coupled to Avalanche Photo Diodes (APDs). As with the silicon detector, the scintillators are cylindrically arrayed around the trap axis just outside of the octupole magnet. To measure the size of a $\bar{p}$ cloud, we first transfer it into an electrostatic well in the octupole field region; the octupole field is turned off during the transfer. We then measure the $\bar{p}$'s

Octupole Off   Octupole On
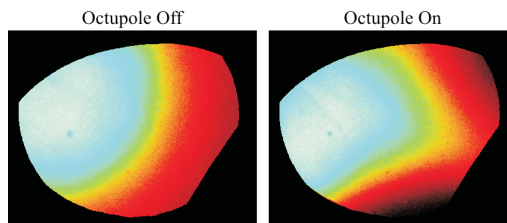
FIGURE 7. Field lines imaged by passing a circular e^- plasma through the octupole with the octupole off and on. Apertures [11] form the image boundaries and limit us to viewing only one quadrant of the octupole field map. The distortion evident in the right-hand image corresponds to one of the flutes at the end of the magnetic surface shown in Fig. 6.

101
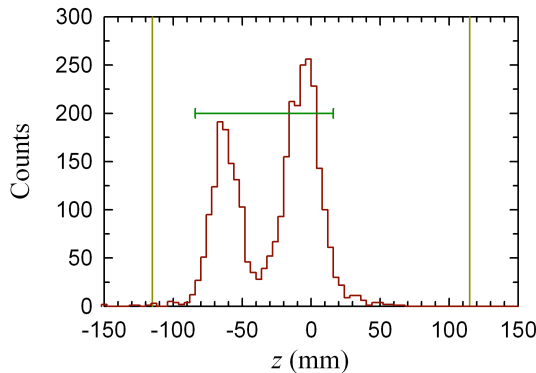
FIGURE 8. Axial positions where the p̄'s hit the trap wall under the influence of the octupole. The horizontal bar indicates the the axial extent and position of the electrostatic well confining the p̄'s. The loss is greatest near the ends of the confining electrostatic well. The positions are determined by a position-sensitive particle detector which monitors the p̄ annihilation products; the vertical bars indicate the axial extent of the detector.

kinetic energy by monitoring the rate at which the p̄'s escape as we slowly lower one endwall of the electrostatic well [22]. Typically we find that the energy is between 1 and 15 eV; the energy depends on the details of the transfer process and the electrostatic well potentials. This measurement is destructive, but since the energy is largely set by the electrostatics, not by the p̄ radial profile, it is sufficient to measure this energy once for a series of profile measurements. From this energy, we determine the bounce length L of the p̄'s in the electrostatic well. The uncertainty (and spread) of the p̄ energy sets the uncertainty in the orbit lengths. Finally, for each p̄ cloud that we want to analyze, we slowly ramp up the octupole field B_w while monitoring the losses. From the time history of the losses, we can invert Eq. (1) to reconstruct the radial distribution of p̄'s.

We have verified that, for identically prepared p̄ clouds, the reconstructed profile is independent of the electrostatic well shape and length, and the octupole ramp time [18]. The data for the latter test are shown in Fig. 9.

We have used our new diagnostic to characterize our p̄ manipulation sequences, and to study interesting physics issues. An example is shown in Fig. 10, where we show radial profiles for a mixed e^+-p̄ plasma. As the density of the e^+ plasma is increased, p̄'s appear to be transported outward. The interpretation of these results is complicated by cooling of the p̄'s on the e^+'s. Cooling will cause some charge to appear at falsely low radii, and this very likely causes us to underestimate the outward movement of the p̄'s.

A possible explanation of the outward movement shown in Fig. 10 is that it is the result of the formation of highly excited H̄ that is either 1) ionized at the radial edge of the e^+ plasma by its self consistent electric field, where the field is strongest, or 2) ionized by the vacuum electrostatic well fields. Note that the p̄'s from H̄ that was ionized within the e^+ plasma radius would have the opportunity to recombine into H̄ again, while those at larger radii would orbit unperturbed. With time, the p̄'s remaining in the e^+ plasma would be swept out to larger radii. Unpublished simulations of realistic

102
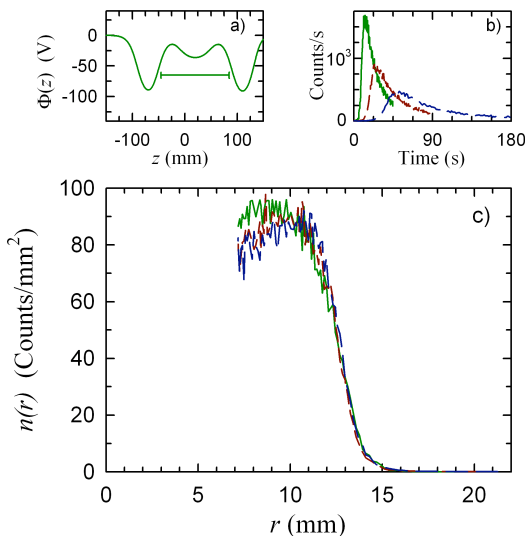
FIGURE 9. Comparison of the radial profiles with octupole ramps of 45 (green solid), 90 (red short-dash), and 180 s (blue long-dash). Panel a) shows the electrostatic well potential $\Phi(z)$; the horizontal bars indicate the 130 ± 5 mm axial extent and position of the $\overline{p}$ orbits before the application of the octupole field. Panel b) shows the time history of the $\overline{p}$ annihilations as the octupole field is ramped up. Panel c) shows the resulting radial profiles. The maximum B_w at the end of the ramp was 1.54 T, and $B_z = 1.03$ T.

antihydrogen formation/field ionization cycles, using the code described in [23], found similar transport. We do not yet have any other direct experimental evidence that this cycling occurs.

CONCLUSIONS

In this paper, we report detailed measurements of trapped $\overline{p}$ radial compression [11]. We can compress the $\overline{p}$ density by a factor of ten and decrease their radii to 0.29 mm. These clouds are 10-20 times smaller in radius than the clouds reported by ATHENA [21] and ATRAP [24]. Control of the radial profile of the $\overline{p}$'s is critical to their survival in a Minimum-B trap. We have also studied the effect of the e^- plasma radius on the cooling of hot $\overline{p}$'s. Finally, we have developed [11, 18] diagnostics that give the detailed radial profile of $\overline{p}$'s near the trap axis, and from about 7 mm to the trap wall.

ACKNOWLEDGMENTS
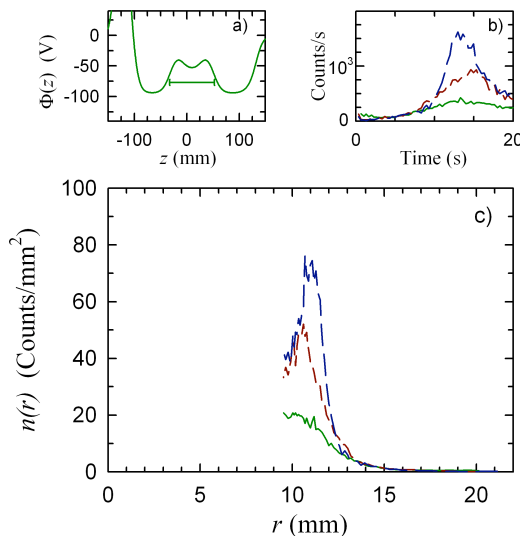
FIGURE 10. Comparison of the $\bar{\text{p}}$ radial profile with different density positron plasmas. The green, solid curve shows the profile with no e^+, and the red short-dash and blue long-dash curves show the profile with 13 million and 25 million e^+ respectively. The well length was 85 ± 5 mm, the maximum field was 1.20 T, and the ramp time was 20 s. The graph descriptions and all other parameters are the same as in Fig. 9.

REFERENCES

1. G. Andresen, W. Bertsche, A. Boston, P. D. Bowe, C. L. Cesar, S. Chapman, M. Charlton, M. Chartier, A. Deutsch, J. Fajans, M. C. Fujiwara, R. Funakoshi, D. R. Gill, K.Gomberoff, J. S. Hangst, R. S. Hayano, R. Hydomako, M. J. Jenkins, L. V. Jørgensen, L. Kurchaninov, N. Madsen, P. Nolan, K. Olchanski, A. Olin, A. Povilus, F. Robicheaux, E. Sarid, D. M. Silveira, J. W. Storey, H. H. Telle, R. I. Thompson, D. P. van der Werf, J. S. Wurtele, and Y. Yamazaki, *Phys. Rev. Lett.* **98**, 023402 (2007).
2. G. Gabrielse, P. Larochelle, D. L. Sage, B. Levitt, W. S. Kolthammer, I. Kuljanishvili, R. McConnell, J. Wrubel, F. M. Esser, H. Glückler, D. Grzonka, G. Hansen, S. Martin, W. Oelert, J. Schillings, M. Schmitt, T. Sefzick, H. Soltner, Z. Zhang, D. Comeau, M. C. George, E. A. Hessels, C. H. Storry, M. Weel, A. Speck, F. Nillius, J. Walz, and T. W. Hänsch, *Phys. Rev. Lett.* **98**, 113002 (2007).
3. D. E. Pritchard, *Phys. Rev. Lett.* **51**, 1336 (1983).
4. J. Fajans, W. Bertsche, K. Burke, S. F. Chapman, and D. P. van der Werf, *Phys. Rev. Lett.* **95**, 155001 (2005).
5. J. Fajans, W. Bertsche, K. Burke, A. Deutsch, S. F. Chapman, K. Gomberoff, D. P. van der Werf, and J. S. Wurtele, "Simple loss scaling laws for quadrupoles and higher-order multipoles used in antihydrogen traps," in *Non-Neutral Plasma Physics VI: Workshop on Non-Neutral Plasmas*, edited by M. Drewsen, U. Uggerhøj, and H. Knudsen, AIP, Melville, N.Y., 2006, vol. 862, p. 176.
6. J. Zhang, C. L. Taylor, and F. Robicheaux, *J. Phys. B* **40**, 1019 (2007).
7. J. Fajans, and A. Schmidt, *Nucl. Instr. Meth. Phys. Res. A* **521**, 318 (2004).
8. Y. Yamazaki, *Hyperfine Interactions* **138**, 141 (2001).
9. N. Kuroda, H. A. Torii, M. Shibata, Y. Nagata, D. Barna, D. Horváth, M. Hori, J. Eades, A. Mohri, K. Komaki, and Y. Yamazaki, "Control of plasmas for production of ultraslow antiproton beams," in *Physics with Ultra Slow Antiproton Beams*, edited by Y. Yamazaki, and M. Wada, American Institute

of Physics, Wako, Japan, 2005, vol. CP793, p. 307.

10. H. A. Torii, N. Kuroda, M. Shibata, Y. Nagata, D. Barna, M. Hori, A. Mohri, K. Komaki, and Y. Yamazaki, "Extraction of ultra-slow antiproton beams and their physics application," in *Low Energy Antiproton Physics-LEAP '05*, edited by D. Grzonka, R. Czyzykiewicz, W. Oelert, T. Rozek, and P. Winter, Amer. Inst. of Physics, 2005, vol. CP796, p. 413.

11. G. Andresen, W. Bertsche, P. D. Bowe, C. C. Bray, E. Butler, C. L. Cesar, S. Chapman, M. Charlton, J. Fajans, M. C. Fujiwara, R. Funakoshi, D. R. Gill, J. S. Hangst, W. N. Hardy, R. S. Hayano, M. E. Hayden, R. Hydomako, M. J. Jenkins, L. V. Jørgensen, L. Kurchaninov, R. Lambo, N. Madsen, P. Nolan, K. Olchanski, A. Olin, A. Povilus, P. Pusa, F. Robicheaux, E. Sarid, S. S. E. Nasr, D. M. Silveira, J. W. Storey, R. I. Thompson, D. P. van der Werf, J. S. Wurtele, and Y. Yamazaki, "Compression of antiproton clouds for antihydrogen trapping" (2008), submitted to Phys. Rev. Lett.

12. M. Amoretti, C. Amsler, G. Bonomi, A. Bouchta, P. Bowe, C. Carraro, C. Cesar, M. Charlton, M. J. T. Collier, M. Doser, V. Filippini, K. S. Fine, A. Fontana, M. C. Fujiwara, R. Funakoshi, P. Genova, J. S. Hangst, R. S. Hayano, M. H. Holzscheiter, L. V. Jørgensen, V. Lagomarsino, R. Landua, D. Lindelöf, E. Lodi-Rizzini, M. Macrì, N. Madsen, G. Manuzio, M. Marchesotti, P. Montagna, H. Pruys, C. Regenfus, P. Riedler, J. Rochet, A. Rotondi, G. Rouleau, G. Testera, A. Variola, T. L. Watson, and D. P. van der Werf, *Nature* **419**, 456 (2002).

13. G. Gabrielse, N. S. Bowden, P. Oxley, A. Speck, C. H. Storry, J. N. Tan, M. Wessels, D. Grzonka, W. Oelert, G. Schepers, T. Sefzick, J. Walz, H. Pittner, T. W. Hänsch, and E. A. Hessels, *Phys. Rev. Lett.* **89**, 213401 (2002).

14. G. Gabrielse, X. Fei, L. A. Orozco, R. L. Tjoelker, J. Haas, H. Kalinowsky, T. A. Trainor, and W. Kells, *Phys. Rev. Lett.* **63**, 1360 (1989).

15. A. J. Peurrung, and J. Fajans, *Rev. Sci. Instrum.* **64**, 52 (1993).

16. X.-P. Huang, F. Anderegg, E. M. Hollmann, C. F. Driscoll, and T. M. O'Neil, *Phys. Rev. Lett.* **78**, 875 (1997).

17. R. G. Greaves, and C. M. Surko, *Phys. Rev. Lett.* **85**, 1883 (2000).

18. G. Andresen, W. Bertsche, P. D. Bowe, C. C. Bray, E. Butler, C. L. Cesar, S. Chapman, M. Charlton, J. Fajans, M. C. Fujiwara, R. Funakoshi, D. R. Gill, J. S. Hangst, W. N. Hardy, R. S. Hayano, M. E. Hayden, A. J. Humphries, R. Hydomako, M. J. Jenkins, L. V. Jørgensen, L. Kurchaninov, R. Lambo, N. Madsen, P. Nolan, K. Olchanski, A. Olin, A. Povilus, P. Pusa, F. Robicheaux, E. Sarid, S. S. E. Nasr, D. M. Silveira, J. W. Storey, R. I. Thompson, D. P. van der Werf, J. S. Wurtele, and Y. Yamazaki, "A novel antiproton radial diagnostic based on octupole induced ballistic loss" (2008), submitted to Phys. Plasmas.

19. J. Fajans, N. Madsen, and F. Robicheaux, "Critical loss radius in a Penning trap subject to multipole fields" (2008), submitted to Phys. Plasmas.

20. M. Fujiwara, "Detecting antihydrogen: the challenges and the applications," in *Physics with ultra slow antiproton beams*, edited by Y. Yamazaki, and M. Wada, AIP, Wako, Japan, 2005, vol. 793, p. 111.

21. M. C. Fujiwara, M. Amoretti, G. Bonomi, A. Bouchta, P. D. Bowe, C. Carraro, C. L. Cesar, M. Charlton, M. Doser, V. Filippini, A. Fontana, R. Funakoshi, P. Genova, J. S. Hangst, R. S. Hayano, L. V. Jørgensen, V. Lagomarsino, R. Landua, E. Lodi-Rizzini, M. Marchesotti, M. Macri, N. Madsen, G. Manuzio, P. Montagna, P. Riedler, A. Rotondi, G. Rouleau, G. Testera, A. Variola, D. P. van der Werf, and Y. Yamazaki, *Phys. Rev. Lett.* **92**, 65005 (2004).

22. M. Amoretti, C. Amsler, G. Bonomi, A. Bouchta, P. D. Bowe, C. Canali, C. Carraro, C. L. Cesar, M. Charlton, M. Doser, V. Filippini, A. Fontana, M. C. Fujiwara, R. Funakoshi, P. Genova, J. S. Hangst, R. S. Hayano, L. V. Jørgensen, A. Kellerbauer, V. Lagomarsino, R. Landua, D. Lindelof, E. L. Rizzini, M. Macrí, N. Madsen, G. Manuzio, P. Montagna, H. Pruys, C. Regenfus, A. Rotondi, G. Testera, A. Variola, L. Venturelli, D. P. van der Werf, and Y. Yamazaki, *Phys. Lett. B* **590**, 133 (2004).

23. F. Robicheaux, *Phys. Rev. A* **70**, 022510 (2004).

24. P. Oxley, N. S. Bowden, R. Parrott, A. Speck, C. H. Storry, J. N. Tan, M. Wessels, G. Gabrielse, D. Grzonka, W. Oelert, G. Schepers, T. Sefzick, J. Walz, H. Pittner, T. W. Hänsch, and E. A. Hessels, *Phys. Lett. B* **595**, 60 (2004).